Wavelet Analysis of Coherent Structures at the Atmosphere–Forest Interface*

W. GAO

Environmental Research Division, Argonne National Laboratory, Argonne, Illinois

B. L. LI

Center for Biosystems Modelling, Department of Industrial Engineering, Texas A&M University, College Station, Texas

(Manuscript received 31 December 1992, in final form 19 April 1993)

ABSTRACT

Wavelet analysis was applied to turbulence data for temperature and vertical velocity within and above a deciduous forest. This method appears to provide an objective technique for examining thermal and flow fields associated with coherent structures occurring near the forest. The two-dimensional unfolding in time and scale by the wavelet transform illustrates discrete warm and cool centers associated with organized updrafts and downdrafts, which have similar patterns but different magnitudes at different heights. Wavelet variances computed for temperature and velocity at different heights appear to have local maximum values corresponding to certain time scales, which are self-consistent and useful for objective determination of the principal time scale of the structures. Within the canopy, the principal time scales of the structures determined by this technique are 56–60 s and 40–44 s for the temperature and vertical velocity fields, respectively. These time scales are close to those determined by the multilevel detection scheme used in a previous analysis. The temperature structures above the canopy have a shorter duration, but the rate of the decrease in the time scale with increasing height appears to be proportional to the increase in mean wind speed. The horizontal size of the structure determined by the product of local wind speed and the detected principal time scales is in the range of 83–112 m. The time scale of the structures identified in vertical velocity appears to be consistently smaller than that in the thermal field. The canopy structures show a smooth connection in the scale change with circulations of lower frequency (about 5–7 min) and merge into updrafts and downdrafts of these larger-scale circulations.

1. Introduction

Atmosphere–forest exchanges contribute important surface sources and sinks to atmospheric circulations of momentum, heat, water vapor, and trace gases. The exchange processes are dynamically controlled by the nature of the turbulence in the region within and immediately above the canopy, in addition to plant biophysical factors. A large number of theoretical and observational studies have shown that the turbulent transfer in this region is distinctively different from that in the atmospheric surface layers over a short canopy or smooth ground. For example, observations by Garratt (1978) and Raupach (1979) showed that the turbulent flux measured above a forest canopy can be greater by a factor of 2 than that predicted by flux gradient relations describing diffusion in the atmospheric surface layer. The transport in this roughness sublayer tends to be far more efficient than gradient diffusion models would describe. Some advanced approaches such as high-order closure models and Lagrangian diffusion models have been developed to improve numerical description of turbulent transport in the near-canopy regions (Wilson and Shaw 1977; Meyers and Paw U 1986, 1987; Raupach 1987; Baldocchi 1992), although the mechanism of the transport process is still not fully understood (Gao et al. 1989; Shaw and Schumann 1992).

Intermittent, organized features of canopy flow have been given increased attention and examined by a number of investigators for different canopies. Finnigan (1979), Raupach (1981), Shaw et al. (1983), and Baldocchi and Meyers (1988) applied a conditional analysis technique to data from wheat, simulated wind tunnel canopies, corn, and forest, respectively. They used quadrant analysis to decompose flux contributions by different types of motion, demonstrating that intensified transfer can occur within some short-lived events and can carry a significant portion of the total flux near the canopy.

Recent efforts of Gao et al. (1989) and Bergström and Högström (1989) illustrated two-dimensional distributions of velocity and scalar fields associated with

* This work was supported by the U.S. Department of Energy, Office of Energy Research, Office of Health and Environmental Research, under Contract W-31-109-Eng-38.

Corresponding author address: Dr. Weigang Gao, Bldg. 203, Rm J152, Argonne National Laboratory, 9700 South Cass Ave., Argonne, IL 60439.

coherent structures near forest canopies. Gao et al. (1989) showed that the coherent structures are characteristic of repeated and well-organized cycles of ejectionlike upwelling flow and the subsequent sweeplike descending motions. The organized ejections and sweeps can produce much more efficient transport than local turbulence, creating sharp temperature and humidity microfronts between the two flows, under lapse conditions and within and above a transpiring canopy. The ejection is weaker and lasts longer than the sweep, and the two flows tend to have similar magnitudes and durations at about twice the canopy height (Gao et al. 1991).

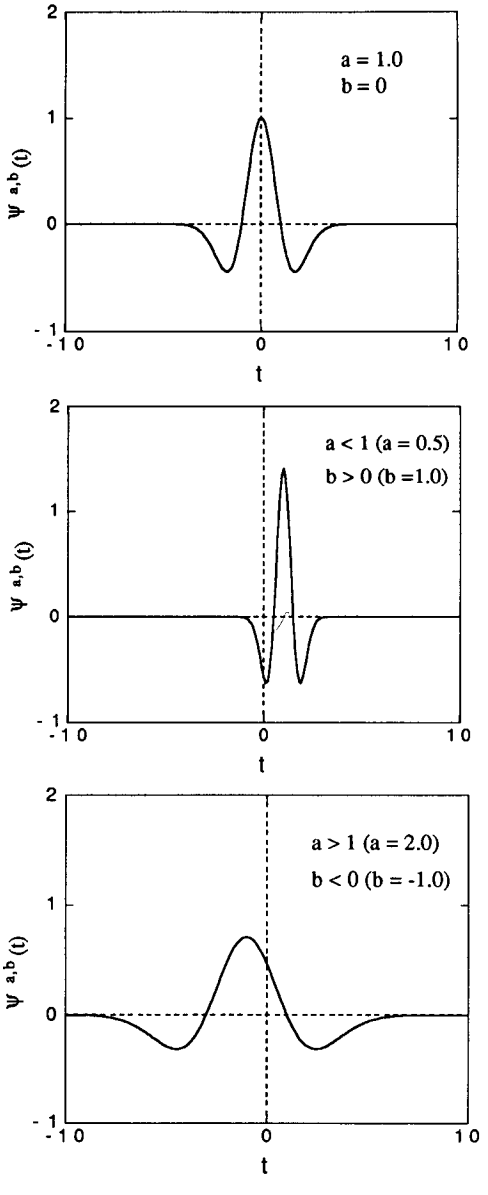

FIG. 1. Changes in the shape of the wavelet function $\psi^{a,b}(t)$ with selected values of a and b for the "mother wavelet" given by the "Mexican hat" function $\psi(t') = (1 - t'^2)\exp(-t'^2/2)$.

Using a multilevel detection scheme with a relatively large number of datasets, Gao et al. (1991, 1992) demonstrated that canopy coherent structures can occur in unstable and near-neutral atmospheric conditions and have a mode time interval of about 50 s between consecutively occurring microfronts. The surface pressure measured on the forest floor follows a characteristic change during the occurrence of the canopy coherent structure, as shown by Shaw et al. (1990) and Gao et al. (1992). The change, according to Shaw et al. (1990), can be dynamically related to the flow fields of the structure and provides additional understanding of the dynamics of the structure. Recently, Shaw and Schumann (1992) used a large-eddy simulation to study the coherent structure in the canopy layer.

To identify the coherent structures from data taken in field experiments and to examine their frequency and dynamics, choosing an objective detection technique becomes crucial because the signal representing the structure can be very irregular over time and disturbed by high-frequency background turbulence to varying degrees. Some single-layer conditional sampling schemes, such as the variable interval time average (VITA) (Blackwelder and Kaplan 1976; Chen and Blackwelder 1978; Schols 1984; Shaw et al. 1989), quadrant analysis (Grass 1971; Finnigan 1979; Raupach 1981; Shaw et al. 1983; Baldocchi and Meyers 1988), and pattern recognition (Wallace et al. 1977) have been developed for the detection of coherent structures. However, the detection of coherent structures with these techniques often requires the selection of time interval and threshold criteria suitable for specific data. The objective determination of these criteria usually is difficult, and chosen values may influence the detection results. Wavelet analysis, a relatively new mathematical method, provides both scale and time information of analyzed signals and allows an objective separation of different structures at different time scales at different times. In the present paper, we apply wavelet analysis to the turbulence data acquired within and above a deciduous forest to examine the spatial and scale characteristics of the coherent structure in the region.

2. Wavelet theory

Wavelet analysis is a mathematical method introduced recently by Morlet et al. (1982), Morlet (1983), and Grossmann and Morlet (1984). The more recent development in its theories, mathematics, and applications can be found in Grossmann (1986), Daubechies (1988), Argoul et al. (1989), Mallat (1989a and b), Mallat and Zhong (1992), Chui (1992), and Daubechies (1992). Farge (1992) gave a comprehensive review on the application of wavelet analysis to turbulence study. The wavelet transform is similar to the windowed Fourier transform but has a few significant differences. In the wavelet transform, the shape of the

basic wavelet function in the time domain varies with frequency to provide an improved fitting to nonlinear, irregular data. In addition, the wavelet analysis provides both scale and time information and allows one to separate and sort different structures on different time scales at different times, or on different spatial scales at different locations.

The integral wavelet transform is defined by

$$(W_\psi f)(a, b) = \frac{1}{|a|^{1/2}} \int f(t)\psi\left(\frac{t-b}{a}\right)dt, \quad (1)$$

where the function $\psi^{a,b}(t) = |a|^{-1/2}\psi[(t-b)/a]$ is called the "wavelet," and the function $\psi[(t-b)/a]$ is called "mother wavelet." The parameters a ($a \neq 0$) and b are used to adjust the shape and location of the wavelets, respectively. The $|a|^{-1/2}$ term keeps the energy of the scaled wavelet equal to the energy of the original mother wavelet. As Fig. 1 shows, as a changes, the shape of wavelet $\psi^{a,b}(t)$ is compressed or stretched to cover different frequency ranges; that is, a large a value corresponds to a small frequency or a large scale. Changing b allows one to move the time localization center and translate wavelets through all data points. In this way, the wavelet transform (1) provides a time-frequency description of raw data $f(t)$. In contrast to the windowed Fourier transform, the shapes of the wavelet $\psi^{a,b}(t)$ have time widths that can adapt to their frequency, with a very narrow shape associated with a high-frequency $\psi^{a,b}(t)$ and a much wider shape with a low-frequency $\psi^{a,b}(t)$, but the area of the window is a constant. Thus, the wavelet transform has an improved ability to "zoom in" and "zoom out" to structures at different scales.

In the present study, the "Mexican hat" wavelet function $\psi(t') = (1 - t'^2)\exp(-t'^2/2)$ was used, which is the second-order derivative of the Gaussian function defined within $-4 \leq t' \leq 4$. The basic wavelet window function satisfies the following condition:

$$\int \psi(t')dt' = 0. \quad (2)$$

Here t' is replaced by $(t-b)/a$ when the wavelet function is applied to (1). The condition (2) ensures that the area covered by the wavelet envelope is conserved and that the shape and frequency of the wavelet function can always be correlated while a and b vary. The "Mexican hat" function is well localized in both time and frequency.

The wavelet transform of real data $f(t)$ needs to be computed by restricting a and b to discrete values, which were within the ranges $1 \leq a \leq 225$ and $4a + 1 \leq b \leq n - 4a$ for the present time-series data with a 1-s interval and $t = 1, 2, \cdots, n$, $n = 1800$. The discrete form of (1) can be written as

$$(W_\psi f)(a, b) = \frac{1}{a^{1/2}} \sum f(t)\psi\left(\frac{t-b}{a}\right). \quad (3)$$

Analogous to Fourier analysis, a wavelet variance can be computed from wavelet coefficient fluctuations by integration over b to examine overall contributions by structures at different scales.

3. Data and background information

Turbulence data for temperature and vertical velocity, measured at six heights within and above a deciduous forest in a field experiment during 1986 at Camp Borden, Ontario, Canada, were analyzed with the wavelet transform technique. The experiment and measurement methods were described in detail by Neumann et al. (1988) and Shaw et al. (1988). The forest, composed primarily of aspen and maple, had a mean height of 18 m. The temperature and vertical velocity were sampled at 10 Hz with seven triaxial sonic anemometer/thermometers (Kaijio-Denki Co., Ltd.) at four heights within the canopy (5.9, 10.5, 15.4, 17.6 m) from an 18-m tower and at two heights above the canopy (34.2 and 43.1 m) from a 43-m tower. The data collected between 1400 and 1430 EST 2 October 1986, were used for the present analysis. In early October, the forest leaves had partially fallen, and the canopy leaf area index was estimated to be approximately 1.6. The atmosphere on this day was slightly unstable, with the Monin–Obukhov length computed from the heat fluxes and friction velocity for the canopy top equal to -138 m and the mean wind speed at 18 and 48 m equal to 2.1 and 4.9 m s^{-1}, respectively.

Figure 2 shows a 10-min time series of temperature

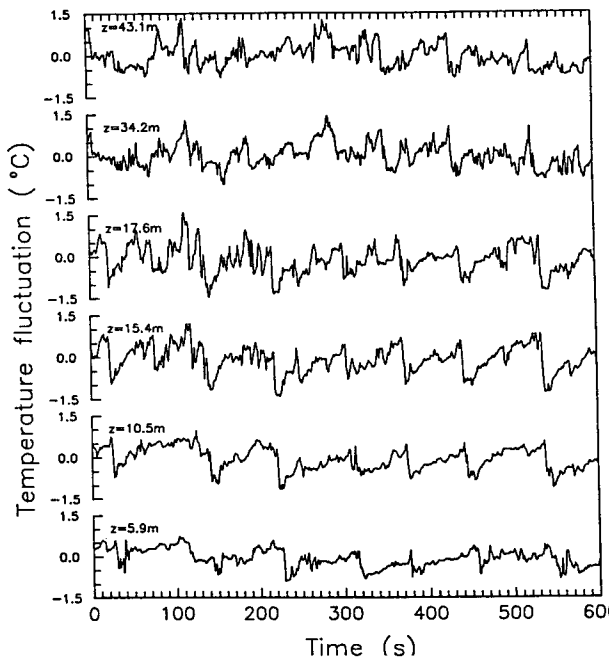

FIG. 2. The 10-min time series of temperature fluctuations measured at different heights within and above an 18-m deciduous forest.

fluctuations at the six heights within and above the canopy, selected from the 30-min time series of the data. As described by Gao et al. (1989) for the same set of data, distinct ramp patterns characterized by a gradual rise followed by a sharp drop of about 1.5°C over a period of 1–3 s can be clearly seen. These temperature ramp structures occur coherently at different heights, but with well-defined time lags. The time–height cross section of temperature contours and velocity vectors (u, w) for a single ramp event from the data is shown in Fig. 3, where the time was plotted backward, and negative and positive times indicate times before and after the microfront, respectively. Figure 3 shows that well-organized structures exist in both thermal and velocity distributions. The thermal field is composed of warm and cool regions separated by a narrow microfront that is tilted along the mean wind direction. Near the canopy top, the vector flow field shows a weak upward motion before the microfront arrives and a strong downward motion after the microfront passes. The upward motions transport warm, moist air from inside the canopy and the downward motion acts to replace the ejected air mass and to bring in cool, dry air from aloft. These organized, nonlocal-scale transports create local temperature fluctuations in a magnitude much greater than would be expected for local, small-scale turbulence. The more detailed features on the two-dimensional fields of the coherent structures, their contributions to total transport, the horizontal translating speed, the surface pressure field, the occurrence frequency, and some aspects of dynamics were described by Gao et al. (1989), Shaw et al. (1989), Shaw et al. (1990), Gao (1990), and Gao et al. (1992).

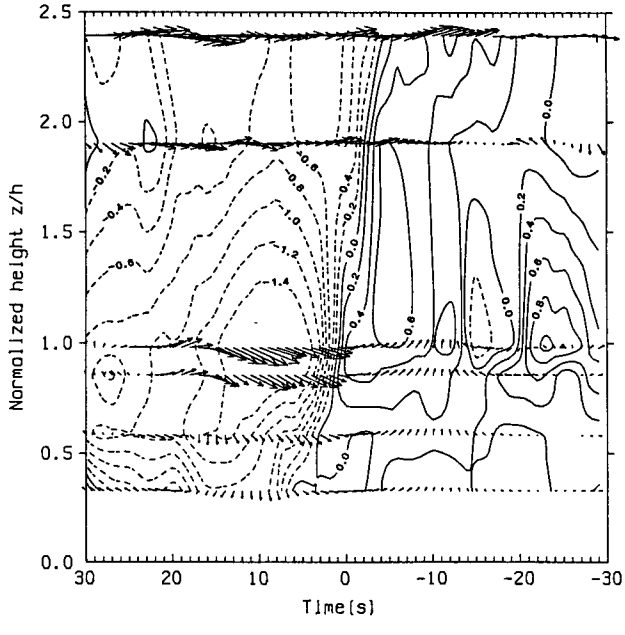

FIG. 3. Temperature contours (lines) and velocity fields (arrows) associated with a single ramp structure. The dashed and solid lines denote the local temperature differences from 30-min means at each height, and the arrows represent the two-dimensional (u, w) wind velocities, with the maximum arrow length representing a magnitude of 5.5 m s^{-1}. Note that time increases from right to left.

4. Temperature structures

The wavelet transform was applied to the total time series of both temperature and vertical velocity measured at six heights within and above the canopy. The original data sampled at 10 Hz were reduced to 1-Hz data by simple block averaging. The data then were processed by using the wavelet transform (3), with the time scales used for sorting different structures defined by the values of $2a$, since a is the half-width of wavelets. Apparently $2a$ varies from 1 to 450 s, because $1 \leqslant a \leqslant 225$. The result for the temperature data at the canopy top is shown in Fig. 4. The upper panel shows values of the wavelet transform function, and the lower panel shows the original time series. Note that the time series in Fig. 2 does not start from the beginning of the data and thus is different from the first part of the time series in Fig. 4. The transform function of temperature is not normalized, and the color coding reflects a default setting suitable for a sufficient visualization of changes.

The disorganized field near the bottom of the upper panel of Fig. 4 is contributed primarily by random background turbulence at very small scales of less than 10 s. As the time scale increases, the distribution tends to be organized into discrete plumelike structures near the time scale of 50 s. These structures are characteristic of strong negative centers in deep blue and occur alternately with positive areas in yellow. The patterns above 50 s gradually merge into a few large negative and positive centers, which we believe correspond to the low-frequency trends appearing in the time series, as they can be seen in the time series plotted immediately below. These low-frequency trends have a time scale on the order of minutes and could be associated with large eddies or thermal plumes penetrating the entire atmospheric boundary layer (ABL).

The discrete plumelike negative centers near the 50-s time scale are indicative of temperature structures at scales intermediate between small-scale turbulence and large-scale ABL structures. The locations of these thermal structures can be easily identified in the color plot of Fig. 4 and are marked by the arrows immediately below. These locations are closely associated with the decreases in the temperature ramps shown in the time series plotted in the same figure. The heights of the organized structures, which indicate the extension of the time scale of the identified structures, appear to vary greatly from one structure to another, and some of them extend to cool regions of the ABL circulations.

Although Fig. 4 shows a smooth transition in the time scale from the organized canopy structures to the low-frequency trends or ABL circulations, the canopy structures appear to occur in both larger-scale warm and cool regions with similar frequencies. From Fig.

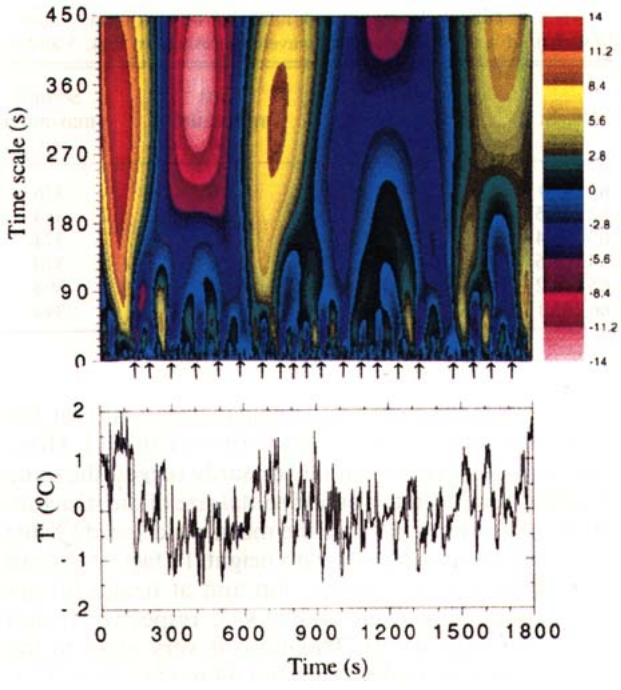

FIG. 4. The 30-min time series of temperature fluctuations (lower panel) and the time and scale distribution of their wavelet transforms (upper panel), which shares the x axis used in the lower panel. The time scale is defined as the $2a$ value. The arrows at the bottom of the upper panel indicate the locations of the temperature structures, identified on the basis of the plumelike negative centers immediately above the arrows. The data are for the canopy top.

4, no clear evidence can be found to indicate whether larger-scale updrafts (warm regions) or downdrafts (cool regions) are more favorable to the generation of the canopy structures. The dynamic connection between ABL circulations and canopy coherent structures is unclear, although Fig. 4 shows the continuation of the scale between the two structures. The organized structure in the canopy layer is likely to be triggered by instability on a scale of several times the canopy height (Raupach et al. 1989) through interactions and combinations of wind shear, canopy friction, and pressure changes (Shaw et al. 1990). The updrafts and downdrafts of the ABL structures may feed energy to the canopy structures below and may tend to maintain a local instability for repeated bursts of coherent ejection and sweep motions.

Wavelet variances were computed by integrating fluctuations of wavelet functions over time for every given time scale. The values of the wavelet variance indicate the relative intensities of structures at different scales. Figure 5 shows changes of the wavelet variance for temperature, computed for different heights within and above the canopy. Within the canopy, at a given time scale, the variance increases in magnitude with increasing height, reflecting the greater temperature fluctuations at the canopy top than near the forest floor, which are largely due to the difference in the vertical temperature gradient (Gao et al. 1989).

At a given height, the wavelet variance increases

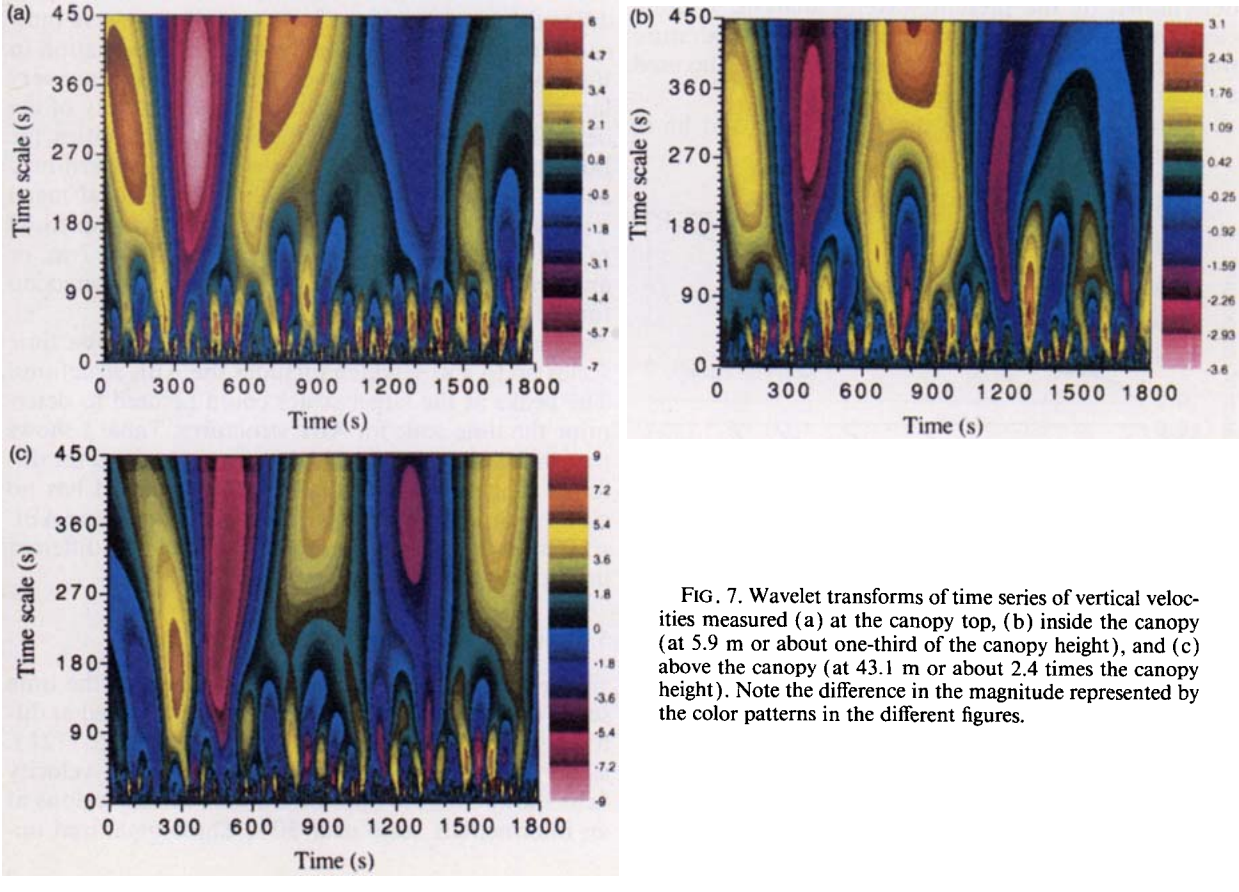

FIG. 7. Wavelet transforms of time series of vertical velocities measured (a) at the canopy top, (b) inside the canopy (at 5.9 m or about one-third of the canopy height), and (c) above the canopy (at 43.1 m or about 2.4 times the canopy height). Note the difference in the magnitude represented by the color patterns in the different figures.

sharply at smaller scales, reaches a maximum value, extends to a plateau associated with a slight decrease, then increases again with increasing scale. This pattern is consistent for all six heights and can be examined by comparing the variance change for h4 in Fig. 5 with the distribution of transformed temperature shown in Fig. 4. The comparison shows that the sharp increase is contributed primarily by the organized temperature structures, which have larger negative and positive centers corresponding to the larger variance values near the time scale of 50 s. The plateau corresponds to the relatively uniform distribution at scales of about 50–90 s in Fig. 4, and the larger-scale deep circulations in Fig. 4 cause the variance to increase at the larger time scales in Fig. 5. The time scale corresponding to the local maximum or the starting point of the plateau, which is defined as the time scale when the first-order derivative of variance with regard to time scale a is equal to zero [i.e., $\partial\ \mathrm{var}(a)/\partial a = 0$], is used to determine the principal time scale of the structures. This scale is representative of a majority of the structures because the further increase in time scale cannot increase the overall variance significantly, as shown by the subsequent plateaus in each curve. This method provides an objective technique for calculating the principal time scale of coherent structures. Within the canopy, this time scale varies between 56 and 60 s (Table 1) and does not differ significantly among different heights, implying that the structures have a similar duration within the canopy. This range of time scales, determined by the present wavelet analysis, is quite close to the mode time interval between temperature microfronts determined by Gao et al. (1992), who used a multilevel detection technique.

At 16 and 25 m above the canopy (h5 and h6 in Fig. 5, respectively), the principal time scale for the organized structure decreases to 26 s (Table 1). However, this decrease does not necessarily suggest the same magnitude of decrease in horizontal size of the structure above the canopy, because the mean wind speed (Table 1) there increases rapidly with height. In fact, the mean wind speeds at the canopy top and at height h6 are approximately 2.0 and 4.0 m s^{-1}, respectively, and their ratio thus is 2.0. This ratio is very close to the ratio of the time scales at 18 and 43 m (56/26 = 2.2), suggesting that the structure may be translated by the local mean wind in the region from the canopy top to about 2.4 times the canopy height and that the horizontal width of the structures may not change much with height.

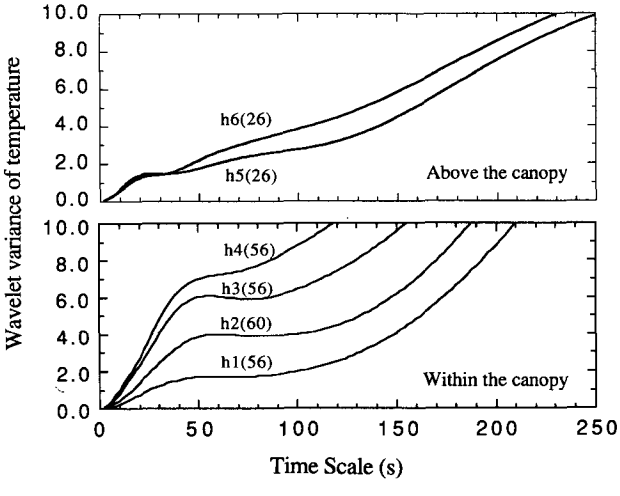

FIG. 5. Changes in the wavelet variance of temperature with the time scale at different heights, where h1 = 5.9 m, h2 = 10.5 m, h3 = 15.4 m, h4 = 17.6 m, h5 = 34.2 m, and h6 = 43.1 m. The numbers inside the parentheses represent the time scale corresponding to the local maximum variances at the beginning of the plateau of each curve, which are also shown in Table 1.

TABLE 1. Time scales (s) corresponding to the maximum values [$\partial\ \mathrm{var}(a)/\partial a = 0$] of temperature wavelet variances in Figs. 5 and 6.

Height (m)	Wind speed (m s^{-1})	First maximum (s)	Second maximum (s)
h1 (5.9)	0.65	56	376
h2 (10.5)	0.86	60	384
h3 (15.4)	1.57	56	374
h4 (17.6)	1.97	56	370
h5 (34.2)	3.18	26	394
h6 (43.1)	4.02	26	394

The principal time scale for h5 appears to be identical to that at h6 although the wind speeds at the two heights differed by about 1 m s^{-1}. As one of reviewers indicated, this may be associated with vertical variation in the structure's size. However, the difference is not very large and it may also be caused by uncertainty of the detection scheme. Considering these uncertainties, the horizontal scales of the ramp structures, determined as the product of the time scale and the local mean wind speed in the region from the canopy top to 43 m, are estimated to be in the range of 83–112 m, or an average value of 100 m, according to the detection for the three heights of h4, h5, and h6.

Figure 6 shows the wavelet variance for the time scales up to 450 s, which includes the ABL structures. The peaks at the larger scales could be used to determine the time scale for ABL structures. Table 1 shows that the time scale of ABL structures obtained for different heights ranges from 370 to 394 s and has no clear height dependence, largely because the same ABL structures influence the measurements at different heights.

5. Vertical velocity structures

The same wavelet analysis was applied to the time series of vertical velocity fluctuations measured at different heights. At the canopy top (Fig. 7a, see p. 1721), as for the temperature case, the transformed velocity field shows discrete updraft and downdraft regions at an intermediate scale near 50 s. These organized up-

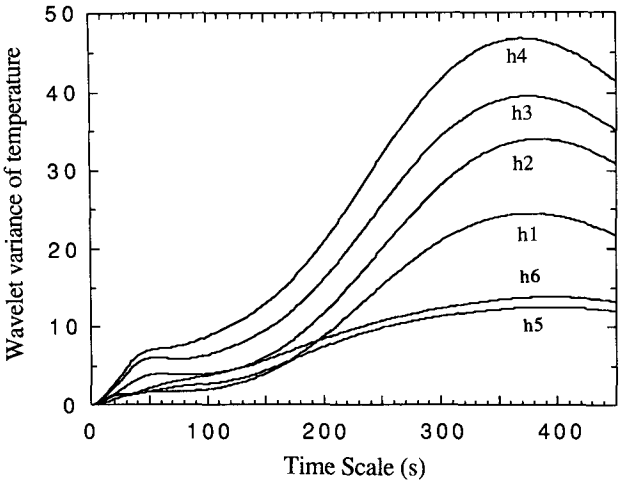

FIG. 6. Same as Fig. 5 but with the time scale extended to 450 s.

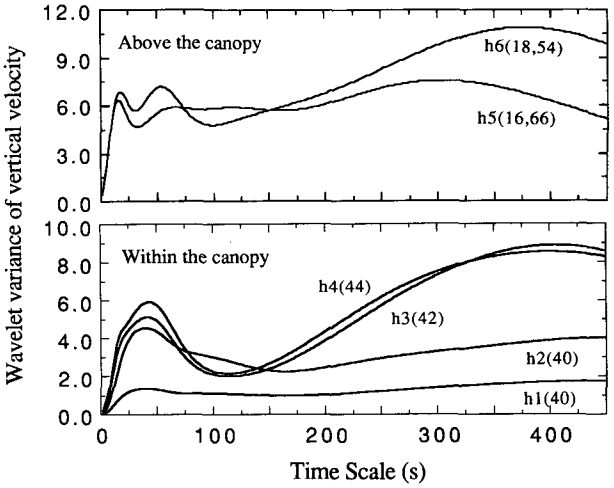

FIG. 8. Same as Fig. 6 but for vertical velocity. The two numbers in the parentheses for h5 and h6 represent the time scales for the first and second maximum variances at each height, which are also shown in Table 2.

drafts and downdrafts can be related to the warm and cool centers identified in Fig. 4 by a close comparison between the two figures. The alternately occurring, organized upwelling and downwelling motions are connected but are not correlated with large-scale patterns, because they occurred in both updrafts and downdrafts of ABL circulations at similar frequencies.

The transformed vertical velocity for the 5.9-m height, which is shown in Fig. 7b, has a distribution similar to that at the canopy top, but the organized structures have updrafts and downdrafts of much smaller magnitudes (note that the color coding changes from Fig. 7a to Fig. 7b). This is because ejections originate near the forest floor with a low momentum and sweeps also have lower vertical velocities when they approach the ground (Gao et al. 1989).

Above the canopy (Fig. 7c for the 43.1-m height), the transformed vertical velocities increase in magnitude and show organized patterns near the time scale of 30 s. Comparison of Fig. 7c with Fig. 7a indicates that the organized updrafts and downdrafts above the canopy have smaller time scales, with most maximum centers located below 20 s, as shown by the deep purple and orange spots near the bottom of Fig. 7c. The transformed vertical velocity within the canopy, however, has most of its positive and negative maximum centers located at a larger scale away from the bottom of Fig. 7a. The difference may be caused by the increase in mean wind speed with height above the canopy, as described above for the thermal field.

The wavelet variance of vertical velocity (Fig. 8) within the canopy has a strong peak near 40–44 s (Table 2), contributed primarily by the organized vertical motions with larger values of wavelet transform functions shown in Fig. 7. This time scale is close to the duration of ejection and sweep determined through conditional analysis by Gao (1990); however, it is smaller than that for thermal structure determined in the previous section. The scale difference between thermal and velocity fields, an important feature of the organized structures in the canopy layer, was also addressed previously (Gao 1990; Gao et al. 1992). The difference can be explained because local temperature changes are effectively produced by the nonlocal transport of vertical gradient by the structures, while local changes of vertical velocity are contributed from both organized motions and their interactions with small-scale turbulence. These interactions can disturb the relatively weak edges of updrafts and downdrafts and reduce the width of well-defined portions of the organized motions. On the other hand, the small-scale disturbances would contribute very little to local temperature changes because of short-distance transport.

At the two heights above the canopy, the wavelet variance of vertical velocity shows some complicated features. At h6, the variances have two peaks at the smaller time scales, one at 18 s and another at 54 s (Table 2). The ratio of the time scale for the canopy top to that for the first peak at h6 is about 2.4, close to the ratio between mean winds at the two heights, which supports our hypothesis that the structure has

TABLE 2. Time scales (s) corresponding to the maximum values $[\partial\ \mathrm{var}(a)/\partial a = 0]$ of vertical velocity wavelet variances in Fig. 8.

Height (m)	First maximum (s)	Second maximum (s)	Third maximum (s)
h1 (5.9)	40	>450	—
h2 (10.5)	40	>450	—
h3 (15.4)	42	404	—
h4 (17.6)	44	398	—
h5 (34.2)	16	66	304
h6 (43.1)	18	54	376

similar horizontal scales at different heights. The time scale for the first peak is smaller than the time scales determined for the thermal fields at the same height. This observation supports the previous understanding that the structure has a larger scale in the thermal field than in the vertical velocity field.

The second peak, which is not as distinctive at h5 as at h6, corresponds to time scales of 66 and 54 s at h5 and h6, respectively. It is not clear whether these second peaks represent the structures in the mixed layer aloft that invade the roughness sublayer or whether they are merely the noise in the data and computation. More analyses are needed to verify this new phenomenon.

6. Conclusions

The wavelet transform was applied to the analysis of characteristics of thermal and velocity fields of coherent structures from turbulence data taken within and above a deciduous forest. The two-dimensional time and scale distribution of transformed fields appears to show discrete, well-organized structures and to allow a relatively objective identification of the coherent structures occurring at different locations. The two-dimensional unfolding by the present wavelet analysis also shows the transition in scale from small-scale random turbulence to larger-scale ABL circulations through the organized structures occurring at intermediate scales.

Changes of wavelet variance with time scale are characterized by a local maximum, which can provide an objective method for determining the principal time scale of the coherent structure. The principal time scales of temperature structures determined by this technique are equal to 56–60 s within the canopy. This range is close to that determined by the multilevel detection scheme used in previous studies (Gao et al. 1992), but wavelet analysis does not require the use of multilevel data and thus provides a more independent determination at each height. At about twice the canopy height, the time scale of the structure determined by the thermal field is shorter (26 s), but the structure appears to have a horizontal size similar to that at the canopy top because of the difference in mean wind speed between the two heights. The horizontal translation speed of the structure may be controlled by the local mean winds at different heights. The horizontal scales of the structures determined by the variance time scale and the local mean wind speed are approximately equal to 83–112 m.

The distribution of vertical velocity in the wavelet transform domain also illustrates discrete, organized updrafts and downdrafts, which have similar patterns but different magnitudes at different heights. The time scales of the structure determined by peak variance for the vertical velocity are 40–44 s within the canopy, shorter than the time scales for the thermal field of the structure in the same region. The scale differences in the thermal and velocity fields may be attributed to the different mechanisms that govern their local changes. The temperature change is caused primarily by nonlocal transport associated with organized updrafts and downdrafts, but the vertical velocity change is influenced by both organized motions and disturbance due to interactions with local turbulence. At about twice the canopy height, the structures of vertical velocity at time scales of 16–18 s contribute a maximum variance. This decrease in time scale is consistent with the increase in mean wind speed at this height.

This study demonstrates the usefulness of wavelet analysis in decomposing structures at different scales hidden in time series data. Using two-dimensional unfolding in both time and scale, the technique (unlike traditional spectral analysis, which can give only a global-mean variance spectrum) provides the location and localized spectrum for structures of interest. This new method is especially useful for studying short-lived transient events such as coherent structures, which are superimposed on background turbulence and cannot be easily identified by conventional statistical techniques.

Acknowledgments. The data used are from the Camp Borden field experiment, which was funded by Environment Canada. Participants included G. den Hartog and H. H. Neumann of the Atmospheric Environment Service, who had overall responsibility for the field experiment; G. Kidd, M. Y. Leclerc, G. Shi, and G. W. Thurtell, University of Guelph, Ontario; and R. H. Shaw, University of California, Davis. This work was supported by the U.S. Department of Energy, Office of Energy, Office of Health and Environmental Research, under Contract W-31-109-Eng-38, as part of research on dry air–surface exchange for the Atmospheric Chemistry Program. Craig Loehle and Richard Coulter provided helpful reviews.

REFERENCES

Argoul, F., A. Arneodo, G. Grasseau, Y. Gagne, E. J. Hopfinger, and U. Frisch, 1989: Wavelet analysis of turbulence reveals the multifractal nature of the Richardson cascade. *Nature*, **338**, 51–53.

Baldocchi, D. D., 1992: A Lagrangian random-walk model for simulating water vapor, CO_2, and sensible heat flux densities and scalar profiles over and within a soybean canopy. *Bound.-Layer Meteor.*, **61**, 113–144.

——, and T. P. Meyers, 1988: Turbulence structure in a deciduous forest. *Bound.-Layer Meteor.*, **43**, 345–365.

Bergström, H., and U. Högström, 1989: Turbulent exchange above a pine forest. II. Organized structures. *Bound.-Layer Meteor.*, **49**, 231–263.

Blackwelder, R. F., and R. E. Kaplan, 1976: On the structure of the turbulent boundary layer. *J. Fluid Mech.*, **76**, 89–112.

Chen, C. P., and R. F. Blackwelder, 1978: Large-scale motion in a turbulent boundary layer: A study using temperature contamination. *J. Fluid Mech.*, **89**, 1–31.

Chui, C. K., 1992: *An Introduction to Wavelets.* Academic Press, 264 pp.

Daubechies, I., 1988: Orthonormal bases of compactly supported wavelets. *Commun. Pure Appl. Math.*, **41**, 909–996.

——, 1992: *Ten Lectures on Wavelets.* SIAM, 357 pp.

Farge, M., 1992: Wavelet transforms and their applications to turbulence. *Annu. Rev. Fluid Mech.*, **24,** 395–457.

Finnigan, J. J., 1979: Turbulence in waving wheat. II: Structure of momentum transfer. *Bound.-Layer Meteor.*, **16,** 213–236.

Gao, W., 1990: Organized turbulence structures and associated transport processes in the lower atmospheric layer within and above a plant canopy. Ph.D. thesis, University of California at Davis, 179 pp. [Available from University Library, UCD, Davis, CA 95616.]

——, and R. H. Shaw, 1992: Conditional analysis of temperature and humidity microfronts and ejection/sweep motions within and above a deciduous forest. *Bound.-Layer Meteor.*, **59,** 35–57.

——, ——, and K. T. Paw U, 1989: Observation of organized structures in turbulent flow within and above a forest canopy. *Bound.-Layer Meteor.*, **47,** 349–377.

——, ——, and ——, 1991: Characteristics of large eddy transport between the lower atmosphere and a deciduous forest. *Proc. 20th Conf. on Agricultural and Forest Meteor.*, Salt Lake City, UT, Amer. Meteor. Soc., 155–157.

Garratt, J. R., 1978: Flux profile relations above tall vegetation. *Quart. J. Roy. Meteor. Soc.*, **104,** 199–221.

Grass, A. J., 1971: Structural features of turbulent flow over smooth and rough boundaries. *J. Fluid Mech.*, **50,** 233–255.

Grossman, A., 1988: Wavelet transform and edge detection. *Stochastic Processes in Physics and Engineering,* P. Blanchard, L. Streit, and M. Hazewinkel, Ed., D. Reidel Publishing Company, 149–157.

——, and J. Morlet, 1984: Decomposition of hardy functions into square integrable wavelets of constant shape. *SIAM J. Math. Anal.*, **15,** 723–736.

Mallat, S., 1989a: Theory for multiresolution signal decomposition: The wavelet representation. *IEEE Trans. Pattern Anal. Mach. Intell.*, **2,** 574–693.

——, 1989b: Multifrequency channel decompositions of images and wavelet models. *IEEE Trans. ASSP,* **37,** 2091–2110.

——, and S. Zhong, 1992: Characterization of signals from multiscale edges. *IEEE Trans. Pattern Anal. Mach. Intell.*, **14,** 710–732.

Meyers, T., and K. T. Paw U, 1986: Testing of higher-order closure model for modeling air flow within and above plant canopies. *Bound.-Layer Meteor.*, **37,** 297–311.

——, and ——, 1987: Modeling the plant canopy micrometeorology with higher-order closure principles. *Agric. For. Meteor.*, **41,** 143–163.

Morlet, J., 1983: Sampling theory and wave propagation. *Acoustic Signal/Image Processing and Recognition,* C. H. Chen, Ed., NATO ASI Series, Springer-Verlag, **1,** 233–261.

——, G. Arens, I. Fourgeau, and D. Giard, 1982: Wave propagation and sampling theory. *Geophysics,* **47,** 203–236.

Neumann, H. H., G. den Hartog, and R. H. Shaw, 1988: Leaf area measurements during leaf-fall for deciduous forest based on hemispheric photographs and leaf-litter collection. *Agric. For. Meteor.*, **45,** 325–345.

Raupach, M. R., 1979: Anomalies in flux-gradient relationships over forest. *Bound.-Layer Meteor.*, **16,** 467–486.

——, 1981: Conditional statistics of Reynolds stress in rough-wall and smooth wall turbulent boundary layer. *J. Fluid Mech.*, **108,** 363–382.

——, 1987: A Lagrangian analysis of scalar transfer in vegetation canopies. *Quart. J. Roy. Meteor. Soc.*, **113,** 107–120.

——, J. J. Finnigan, and Y. Brunet, 1989: Coherent eddies in vegetation canopies. *Proc. Fourth Australasian Conf. on Heat and Mass Transfer,* Christchurch, New Zealand, 75–95.

Schols, J. L. J., 1984: The detection and measurement of turbulent structures in the atmospheric surface layer. *Bound-Layer Meteor.*, **29,** 39–58.

Shaw, R. H., and U. Schumann, 1992: Large-eddy simulation of turbulent flow above and within a forest. *Bound.-Layer Meteor.*, **61,** 47–64.

——, J. Tavangar, and D. P. Ward, 1983: Structure of the Reynolds stress in a canopy layer. *J. Appl. Meteor.*, **14,** 514–521.

——, G. den Hartog, and H. H. Neumann, 1988: Influence on foliar density and thermal stability on profiles of Reynolds stress and turbulence intensity in deciduous forest. *Bound.-Layer Meteor.*, **45,** 391–409.

——, K. T. Paw U, and W. Gao, 1989: Detection of temperature ramps and flow structures at a deciduous forest site. *Agric. For. Meteor.*, **47,** 123–138.

——, ——, X. J. Zhang, W. Gao, G. den Hartog, and H. H. Neumann, 1990: Retrieval of turbulent pressure fluctuations at the ground surface beneath a forest. *Bound.-Layer Meteor.*, **50,** 319–338.

Wallace, J. M., R. S. Brodkey, and H. Eckelmann, 1977: Pattern-recognized structures in bounded turbulent shear flows. *J. Fluid Mech.*, **83,** 673–693.

Wilson, N. R., and R. H. Shaw, 1977: A higher-order closure model for canopy flow. *J. Appl. Meteor.*, **16,** 1198–1205.